RESEARCH ARTICLE

INTERNATIONAL RESEARCH JOURNAL OF MULTIDISCIPLINARY TECHNOVATION

Asian Research Association

DOI: 10.54392/irjmt26325

Analysis on the Electrical Characteristics of Piezoelectric Saw Device for Gas Sensing Applications

S. Bestley Joe [a, *], S. Aaron James [b], S. Maflin Shaby [c], A.S. Augustine Fletcher [a]

[a] SRM Institute of Science and Technology, Vadapalani Campus, Chennai, India
[b] University of Technology and Applied Sciences, Ibri, Oman
[c] Saveetha Institute of Medical and Technical Sciences, Chennai, India
* Corresponding Author Email: bestleyjoe@gmail.com
DOI: https://doi.org/10.54392/irjmt26325
Received: 03-12-2025; Revised: 04-05-2026; Accepted: 18-05-2026; Published: 30-05-2026

Abstract: Piezoelectric material converts the incoming gas wave into acoustic wave for sensing purposes. This research article focusses on the MEMS based surface acoustic wave (SAW) device for gas sensing applications. A key unresolved design in MEMS-based SAW gas sensors is which substrate offers the most suitable balance between resonant-frequency behavior and electrically useful sensing response when the same device structure is used. The SAW device with aluminum interdigitated electrodes (IDT) is covered up using polyisobutylene(PIB) film mounted on a piezoelectric substrate. The PIB layer adsorbs volatile organic compounds (VOC) from air causing shift in resonant frequency caused by underlying piezoelectric material. This causes variation in electrical characteristics like electric field and electric potential which are important parameters connecting electromechanical coupling efficiency. Nine different piezoelectric materials are analyzed for its electrical behaviour. It is observed that $LiNbO_3$, AlN, ZnO and $BaTiO_3$ resulted in good electric field and voltage levels at higher frequency resonance thus proving them to be promising material for gas sensing applications.

Keywords: MEMS, SAW Device, Interdigitated Electrodes, Polyisobutylene, Piezoelectric, Electromechanical Coupling Efficiency.

1. Introduction

Surface acoustic wave (SAW) is a kind of acoustic wave that navigates through the surface of any intermediate medium like solids, water thereby causing them to vibrate. These waves are restricted within a certain region of space where they make changes in physical property that can be detected. The amplitude of the SAW reduces exponentially with respect to distance of propagation on a surface. SAW devices are those which carries the SAW waves and used for detecting any physical phenomenon.

The SAW device is usually a piezoelectric substrate with interdigitated electrodes (IDTs) at the top for attracting physical variables like temperature [1], pressure [2], humidity [3], magnetic field [4], biomolecule [5], chemical concentration [6], stress/strain [7], acceleration [8], viscosity [9] and density [10].

There is a protective outer covering envelope which protects the SAW device from external environment. It is usually a thin film made using either polymer or semiconducting layer. The fixed substrate is a piezoelectric or piezoresistive or capacitive sensing material that supports an acoustic wave propagation. When a piezoelectric substrate is used, it converts the mechanical acoustic waves into electrical waves or vice versa. Such generated waves or electrical signals depend on the physical properties of the substrate used. The comb-shaped structures are the interdigitated electrodes [11] that are embedded on the substrate. Its role is to generate the SAW after it travels across the substrate surface or to generate the surface acoustic wave when an AC voltage is applied. The spacing, number of such electrodes determine the resonant frequency [12] and performance [13] of the SAW device.

MEMS SAW devices and sensors are a dynamic area combining MEMS with acoustic wave propagation to penetrate sensing devices that are highly versatile, compact and sensitive. SAW sensors design, fabrication and application are very vital in recent research due to new material innovation [14], integration with fabrication processes [15], easy wave propagation modeling [16], enhanced sensing mechanisms [17], high temperature and frequency stability [18] followed by multiphysics integration [19].

The figure 1 shows the bar chart representing the increase of the number of publications pertained to SAW devices in science direct and springer journals.

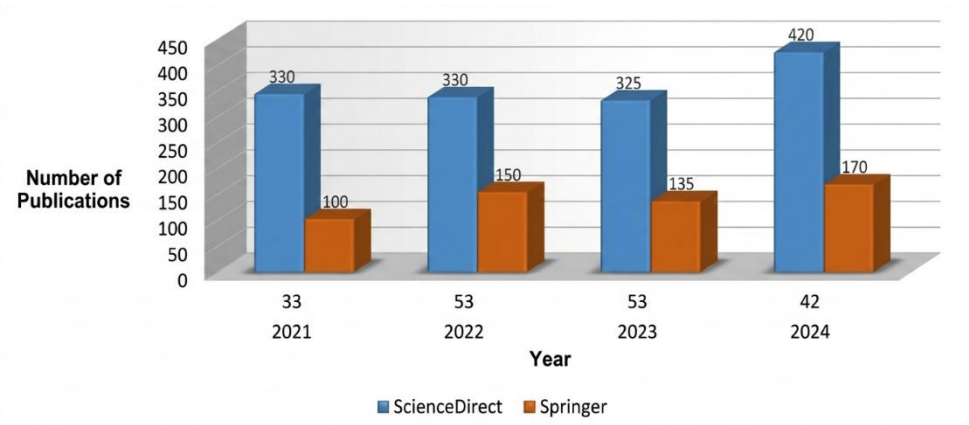

Figure 1. Publication trend in SAW device research

The advanced research work is attributed by the growth in wireless communication as there is a huge demand for reliable and small components to filter and manage signals. SAW devices attracts consumer electronic goods as they are tiny and affordable. It is applied in medical sensors for detection of pathogens and monitoring other health problems as SAW devices are sensitive to physical, chemical and biological changes. When traditional sensors fail to sense reliably temperature, pressure, strain in harsh environment, SAW sensors detect with good reliability.

2. Literature Review

The literature surrounding piezoelectric saw device has evolved through several distinct phases, leading to a diverse array of findings that are often difficult to reconcile in narrative form alone. The table 1 synthesizes these key contributions, highlighting the comparative strengths and limitations of the most influential works in MEMS based SAW devices. In this it is evidenced that SAW devices have diverse application starting from high frequency acoustic wave generation to microfluidics in medical problems. Although many piezoelectric substrates are individually known for SAW operation, substrate selection for gas sensing is still not straightforward because material choice simultaneously affects resonant frequency, electric field and electric potential. As a result, designers often lack a clear basis for deciding whether priority should be given to broad high-field operation, higher frequency operation or surface-potential generation under a common device structure. The distinct contribution of the present work is that it provides a single-framework comparison of nine piezoelectric substrates under the same SAW device configuration, allowing the electrical consequences of substrate selection to be isolated more clearly.

2.1 Sensor Design and Model Description

The heart of the SAW device is the piezoelectric layer whose thickness is 12 µm. When subjected to external gas influence, this layer vibrates and creates surface acoustic waves which travel along the surface. It is indicated by the large orange section as shown in figure 2.

The design and simulation are carried out in COMSOL multiphysics software. The yellow rectangle at the top represents the interdigitated transducer that are made up of aluminum. Each electrode is 1 µm wide whose role is to receive the SAW signals. The green layer present at the top with thickness of 0.5 µm represents Polyisobutylene layer which is a sensitive coating layer often used in SAW sensors for detecting gases. The device total height is 12.5 µm and width is 4 µm. The dimensions reflect the tiny scale of SAW devices making them integrated with microscale devices. The device is modelled and analysed using finite element analysis.

The Polyisobutylene (PIB) is a synthetic polymer formed using polymerization of isobutylene which is a type of alkene [27]. It remains flexible at lower temperature [28] and good stability against acids, ozone and alkalis [29] with good dielectric properties [30]. They are commonly used as tire inner liners and tubes in automotive industry, as sensitive coating layer in gas sensors like SAW and QCM (quartz crystal microbalance), lubricants performing as viscosity modifier in motor oils and also as biocompatible drug delivery materials [31].

In this research work, PIB is used as a sensitive layer that selectively absorbs gas molecules particularly volatile organic compounds (VOCs) [32] The mechanism through which PIB acts in SAW sensors is as follows: PIB adsorbs target gas molecules from air which increases mass of surface layer on SAW device. The added mass causes change in velocity of the surface acoustic wave (SAW). This causes further shift in resonant frequency. The amount of frequency shift [33] is proportional to the gas concentration. The interdigitated electrodes chosen is aluminum due to its excellent conductivity properties [34]. The adjacent surroundings are set to be at room temperature 25^0C and at one atmospheric pressure.

Table 1. Comparison of MEMS SAW device studies

Ref.	Structural framework	Material used	Parameters observed	Work done in brief	Outcome	Application
[13]	Four interdigitated electrodes attached with piezoelectric membrane	PVDF	Resonant frequency, max. sound pressure	Bioinspired MEMS microphone is designed and analyzed for various parameters	Simulation results suggest that designed model suppressed harmonics, increased narrow band properties	Microphone
[20]	Film bulk acoustic resonator (FBAR)	AlN, ZnO, polyimide material electrodes on a Si-substrate	Surface displacement, frequency, impedance, quality factor, coupling coefficient	FBAR is applied with radio frequency signal at top and bottom surfaces resulting in standing wave at certain frequencies	FEA analysis suggests that the polyimide layer with thickness greater than or equal to 9 μm produces confinement of acoustic signal	Acoustic wave sensor
[21]	One port SAW resonator with 100 inter digitated electrodes	Langasite 10 nm, Titanium adhesive layer and 160 nm platinum layer	Displacement, strain, temperature, frequency Vs strain	SAW device designed is subjected to temperature variation with applied strain. The parameters were observed with increasing temperature	High temperature increases the frequency drift and reduces the strain transfer ratio	Temperature sensing
[22]	SAW delay line of 240 μm on a $Y_xAl_{1-x}N$ film with Pt finger pairs per IDT	Wurtzite $Y_xAl_{1-x}N$/ sapphire	Debye temperature density, sound velocities, bulk shear & youngs modulus, coupling factor	The electro acoustic properties of $Y_xAl_{1-x}N$ based SAW sensor is experimented	Performance of the material is proved to be enhanced due to addition of yittrium contents. This is due to significant enhancement of coupling, insertion loss and quality factor	Acoustic SAW resonators
[23]	1D linear array consisting of 3 HBARs (high overtone bulk acoustic resonators)	Si-substrates (400 μm thick, 500 nm wide), AlN stacked between space where material to study is placed	Acoustic pressure distribution at sensing surface, output echo Vs time, acoustic impedance, bulk modulus	SAW sensing surface is subjected to longitudinal acoustic waves and parameters are observed.	The proposed structure is an easy inexpensive approach to manufacture microchannel to carry conductive liquids	Microfluidics biomedical application
[24]	U-type IDT with electrode fingers shaped with letter U (26.5x16) mm^2	Lithium Niobate	Input voltage Vs no load speed, acoustic radiation propulsion (mN), frequency, susceptance, conductance.	SAW device initiated using acoustic radiation propulsion (ARP) is investigated for various analysis which decides	The experimental results suggest that the SAW device initiated using ARP is feasible to be integrated	Micro fluidics

				feasibility of swimmer propulsion system with ARP		
[25]	Top and bottom IDTs (bilayer IDTs) with piezoelectric layer material mounted on a glass substrate	Glass substrate with PVDF-TrFE co polymer	X-ray diffraction curve with intensity, current Vs voltage, scattering parameter Vs frequency	Proposed design of SAW device is fabricated and tested for quality frequency as a notion of increasing the operating frequencies of acoustic waves	The design of SAW device showed a detection frequency as high as 456 MHz. Performance can be improved by incorporating matrix with PVDF- TrFE	High frequency acoustic wave generation
[26]	Pair of straight IDT and pair of focused IDT in a microfluidic channel	$LiNbO_3$ (1 mm thick) substrate with Al layer 200 nm thick electrodes	Cycle number Vs lateral displacement (μm), separation ratio (%)	IDT and FIDT helps separation of tumour cells from RBCs in a blood stream interfaced with SAW	Capable of separating and concentrating 94.2% of polysterene particles using microfluidic channel with diameter of 5 μm	Microfluidics for cancer cell tumour detection

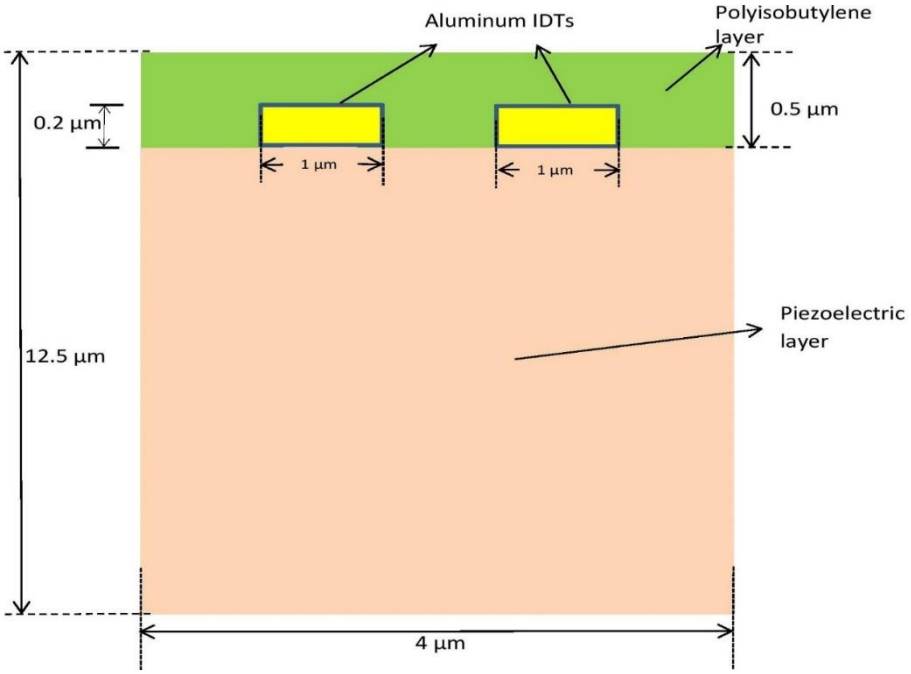

Figure 2. Proposed SAW device schematic

The physics modules included in this research work are solid mechanics and electrostatics. Solid mechanics computes the acoustic wave motion inside the substrate. The modeled SAW device is an electromechanical device in which gas is sensed on the active surface, causing a change in the piezoelectric substrate response and resulting in an equivalent potential variation. Thus, it combines solid mechanics and electrostatics thereby coupling them through the piezoelectric effect. As for as coupling assumptions are concerned, the research work assumes electromechanical coupling only in the $LiNbO_3$ substrate. The substrate is the active piezoelectric medium, the PIB layer is only a passive overlayer with mechanical and dielectric properties and the electrodes are not treated as piezoelectric at all. The second assumption is the 2D plane-strain reduction. The SAW is generated in the plane of the model and any variation out of plane is assumed minimal. The third assumption is the unit-cell periodicity. As practical IDTs have many repeated fingers and each electrode is much longer than its width, edge effects are neglected and thus the whole design is replaced with a single periodic cell. The electrodes are assumed to be equipotential because their electrical conductivity is much higher than that of PIB and $LiNbO_3$. It imposes electrical boundary conditions on the electrode outer boundaries. The left electrode is

grounded, while the right electrode is assigned floating potential with zero surface charge accumulation.

The bottom boundary of the substrate is given a fixed constraint. The two vertical sides use periodic condition in both solid mechanics and electrostatics so that displacements and electric potential are continuous from one side to the other. The SAW device model is meshed with graded distribution of 25 elements with element ratio 25 and reversed direction. This means the mesh is much finer near the top surface and becomes progressively coarser with depth because the displacement is strongest near the surface and decays into the bulk. Eigen frequency solver with parametric sweep is used as the goal is to find resonance frequencies and associated mode shapes. The resonant mode identification method combines physics-based preselection. After solving, the resonant modes are identified by examining the eigenfrequencies and the associated mode shapes.

The structural parameters and material parameters of the SAW device is listed in table 2.

Table 2. Structural and material parameters of the SAW device

Parameters	Value
Air pressure	1 atm
Air temperature	25^0C
Concentration variation of gas	100-200 ppm
Density of PIB	0.918 g/cm^3
Thickness of PIB	0.5 µm or 500 nm
Youngs modulus	10 GPa
Poissons ratio of PIB	0.48
Relative permittivity of PIB	2.2
Rayleigh wave velocity	3488 m/s

In this research work, gas sensing is represented by adsorption-induced mass loading of the PIB sensing film. The analyte concentration in air, c_0(ppm), is converted into molar concentration using the ideal gas law and the absorbed mass concentration in PIB is then calculated as $\rho_{\text{gas, PIB}} = KMc$, where 'K' is the PIB/air partition coefficient, 'M' is the analyte molar mass and 'c' is the gas concentration in mol/m^3[35]. This density is introduced into the piezoelectric eigenfrequency model and the sensing response is quantified as the resulting resonance-frequency shift. In the SAW device structure, only density is altered as the quantity of VOC is changed from 100 to 200 ppm.

Figure 3 shows the 3D schematic of the designed SAW device. The 3D model is obtained by importing the 2D shape and executing extrude operation and choosing the extrusion depth required. The material domains and physics to the new 3D geometry is also reassigned.

All substrate cases are simulated using the same 2D periodic SAW unit-cell geometry with the same electrical and mechanical boundary conditions. Thus, the differences observed in the resonant-frequency and electrical-response results arise from the adopted substrate constitutive properties. The lower boundary of the substrate is fixed while the vertical side boundaries are assigned with periodic conditions for both solid mechanics and electrostatics. The constitutive behaviour of each substrate is defined using its elastic stiffness matrix, piezoelectric coupling matrix, dielectric permittivity tensor and density for each material predefined in COMSOL.

3. Results and Discussion

3.1 Resonant Frequencies

The SAW devices have a piezoelectric substrate that efficiently converts mechanical surface waves to electrical signals at certain frequencies called resonant frequency.

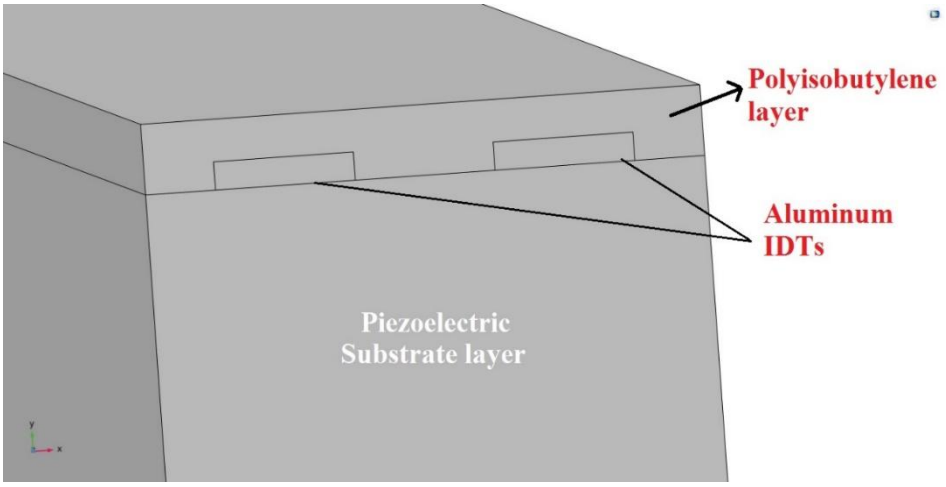

Figure 3. 3D schematic of the SAW device

This value depends upon the piezoelectric material used, its mechanical and electrical properties. Table-3 shows the resonant frequencies of the designed SAW devices using nine different piezoelectric materials.

The widest range is provided by AlN piezoelectric material (378.2-1154.5) MHz that is suitable for broadband applications. Quartz resulted in higher frequency limit (upto 1027 MHz). The SAW device based on $BaTiO_3$, GaAs and PVDF all operate in narrow high frequency range (850-900) MHz. $LiNbO_3$ and PZT provided almost similar resonant frequency characteristics.

3.2 Surface Electric Field Characteristics

In a SAW device, the surface electric field analysis is done in order to optimize and understand its performance while executing the sensing and signal processing operations. Analyzing the surface electric field helps to visualize the electromechanical interaction and thereby evaluating the energy conversion efficiency [36] which helps to manage power, estimate the signal to noise ratio which is a benchmark of improving overall system performance and detection sensitivity. The determination of the magnitude and distribution of surface electric field helps to estimate wave velocity, insertion loss and electromechanical coupling efficiency [37]. This estimation helps to optimize electrode spacing and geometry, determines electrical boundary conditions.

The different piezoelectric material properties can be analyzed by placing them on the piezoelectric substrate layer. Simulation of surface electric field helps to choose optimal piezoelectric material orientation for the desired resonant frequencies and wave modes. This analysis helps to identify the changes taking place at the device level when surface loading or interaction with gases.

Electric field analysis helps to identify of impedance mismatches, reflection points and spurious modes present as a result of surface discontinuities [38].

The table 4 shows the observed maximum and minimum electric fields at resonant frequencies for different piezoelectric SAW substrates. From the analysis it is observed that GaAs and rochelle salt has no electric response and are not viable to be used for SAW devices at test conditions.

High electric fields are exhibited by PVDF, PZT, Quartz and $LiNbO_3$ demonstrating strong and stable electric field generation capabilities. Furthermore, they provide consistent performance across wide frequency range with good field uniformity. $BaTiO_3$ exhibits erratic behaviour revealing positive resonance anomalies and simulation artifacts. $LiNbO_3$ shows a stable performance with few variations specifically at 750.06 MHz ($4.35x10^{-6}$ V/m). Most of the piezoelectric materials show asymmetric maximum and minimum field values indicating built in electric fields due to crystal orientation [39], surface charge effects including field patterns.

The figure 4 shows the surface electric field result of $LiNbO_3$ at 962.47 MHz. It is observed that the maximum electric field is 2.38×10^{-5} V/m and minimum electric field result is 6.93×10^{-10} V/m. The cross-sectional view resembles both surface and bulk field distribution. High field region shown in orange/red lies in the electrode finger space and the field extends approximately (2-3) μm into the substrate.

PVDF material even though being a polymer showed excellent electric field making it suitable for flexible SAW devices and sensors. Quartz showed consistent electric field throughout its space demonstrating broad frequency range.

Table 3. SAW device resonant frequencies

Material	Resonant frequency (MHz)
$LiNbO_3$	660.35, 750.64, 805.63, 942.76, 948.59, 962.47
Quartz	665.3, 850.85, 908.84, 913.66, 943.16, 1027
PVDF	867.19, 868.93, 872.18, 872.83, 873.23, 875.65
Aluminum Nitride	378.2, 628.92, 693.05, 875.42, 1101.4, 1154.5
Rochelle salt	841.79, 841.81, 862.04, 863.84, 877.61, 891.94
Zinc oxide	783.15, 783.53, 843.45, 869.64, 870.24, 920.19
PZT	660.35, 750.64, 805.63, 942.76, 948.59, 962.47
GaAs	822.93, 822.95, 864.14, 865.52, 879.09, 892.87
$BaTiO_3$	856.03, 856.24, 874.54, 874.74, 899.19, 899.3

Table 4. Maximum and minimum electric fields in the SAW device

Material	Resonant frequency (MHz)	Maximum electric field	Minimum electric field
Aluminium Nitride (AlN)	378	3.09×10^{-4} V/m	2.99×10^{-12} V/m
	628	2.99×10^{-4} V/m	2.19×10^{-13} V/m
	693	2.56×10^{-6} V/m	3.06×10^{-11} V/m
	875	2.67×10^{-4} V/m	1.61×10^{-14} V/m
	1101	2.21×10^{-4} V/m	2.57×10^{-13} V/m
	1154	4.35×10^{-6} V/m	8.79×10^{-11} V/m
Barium Titanate ($BaTiO_3$)	856.03	1.92×10^{-5} V/m	3.43×10^{-9} V/m
	856.24	2.27×10^{5} V/m	5.8×10^{-14} V/m
	874.54	1.02×10^{-14} V/m	7.3×10^{-13} V/m
	874.74	5.03×10^{5} V/m	1.26×10^{-8} V/m
	899.1	2.06×10^{-5} V/m	1.08×10^{-15} V/m
	899.3	2.05×10^{-5} V/m	1.29×10^{-10} V/m
Gallium Arsenide (GaAs)	822.93	0 V/m	0 V/m
	822.95	0 V/m	0 V/m
	864.14	0 V/m	0 V/m
	865.52	0 V/m	0 V/m
	879.09	0 V/m	0 V/m
	892.87	0 V/m	0 V/m
Lithium Niobate ($LiNbO_3$)	660.35	2.31×10^{-4} V/m	1.33×10^{-11} V/m
	750.06	4.35×10^{-6} V/m	3.05×10^{-10} V/m
	805	2.12×10^{-4} V/m	2.28×10^{-12} V/m
	942.76	7.82×10^{-5} V/m	3.12×10^{-12} V/m
	948.59	2.1×10^{-4} V/m	3.02×10^{-12} V/m
	962	2.38×10^{-5} V/m	6.93×10^{-10} V/m
Polyvinylidene fluoride (PVDF)	867.19	9.77×10^{-5} V/m	1.13×10^{-11} V/m
	868.93	8.17×10^{-5} V/m	9.64×10^{-6} V/m
	872.1	8.55×10^{-5} V/m	2.35×10^{-12} V/m
	872.8	6.57×10^{-5} V/m	2.66×10^{-8} V/m
	873.23	5.58×10^{-5} V/m	7.96×10^{-9} V/m
	875.65	5.58×10^{-5} V/m	7.96×10^{-9} V/m
Lead Zirconate Titanate (PZT)	660.35	2.31×10^{-4} V/m	1.33×10^{-11} V/m
	750.64	4.35×10^{-6} V/m	3.05×10^{-10} V/m
	805.63	2.12×10^{-4} V/m	2.28×10^{-12} V/m
	942.76	7.82×10^{-5} V/m	3.12×10^{-12} V/m
	948.59	2.1×10^{-4} V/m	3.02×10^{-12} V/m
	962.47	2.38×10^{-5} V/m	6.93×10^{-10} V/m
Quartz	665.3	7.78×10^{-5} V/m	1.38×10^{-12} V/m
	850.85	7.64×10^{-5} V/m	7.24×10^{-14} V/m
	908.84	8.5×10^{-5} V/m	3.77×10^{-13} V/m
	913.66	1.99×10^{-5} V/m	1.39×10^{-10} V/m
	943.16	6.72×10^{-5} V/m	4.75×10^{-12} V/m
	1027	7.46×10^{-5} V/m	3.31×10^{-14} V/m
Rochelle salt	841.7	0 V/m	0 V/m
	841.8	0 V/m	0 V/m
	862.04	0 V/m	0 V/m
	863.84	0 V/m	0 V/m
	877.61	0 V/m	0 V/m
	891.94	0 V/m	0 V/m
ZnO	783.15	1.72×10^{-5} V/m	4.7×10^{-9} V/m
	783.53	2.21×10^{-5} V/m	8.51×10^{-13} V/m
	843.45	2.48×10^{-4} V/m	5.71×10^{-13} V/m
	869.64	1.52×10^{-5} V/m	1.2×10^{-8} V/m
	870.24	3.61×10^{-5} V/m	1.72×10^{-12} V/m
	920.19	6.28×10^{-6} V/m	4.95×10^{-11} V/m

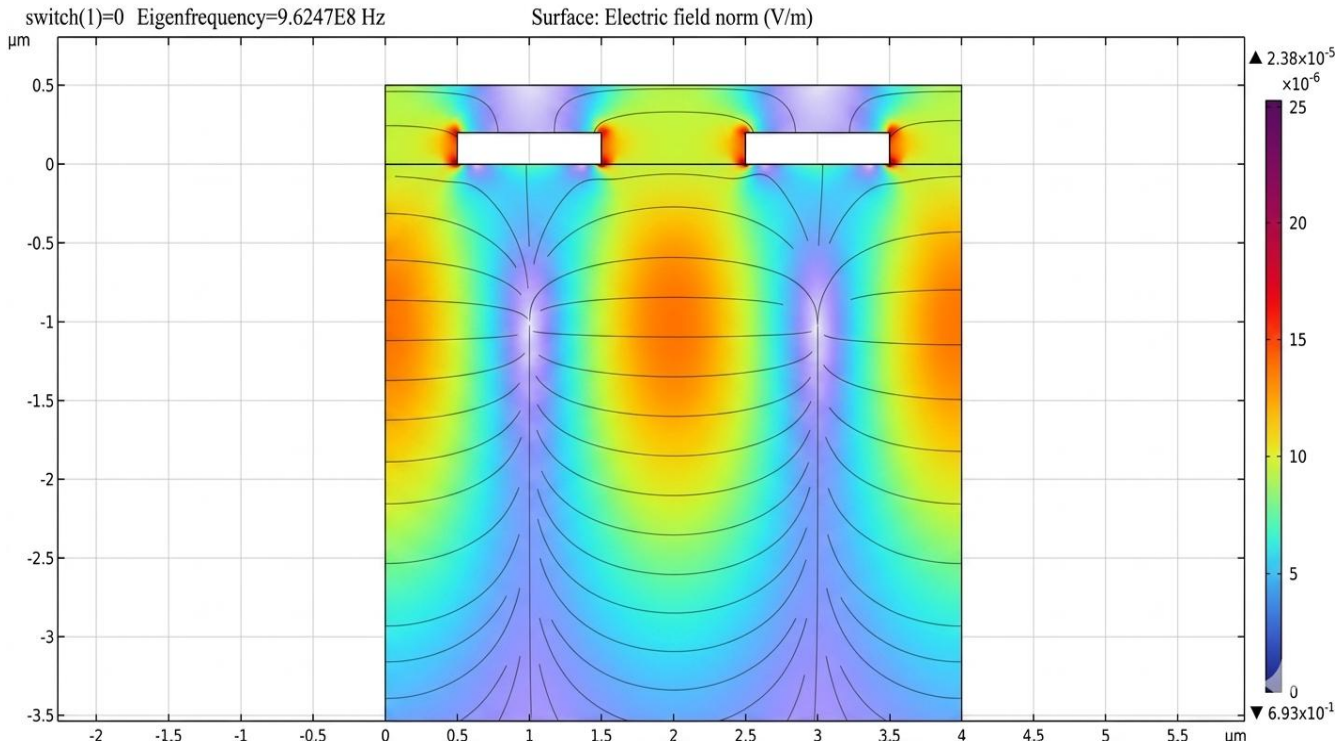

Figure 4. Surface electric field of $LiNbO_3$ at 962.47 MHz

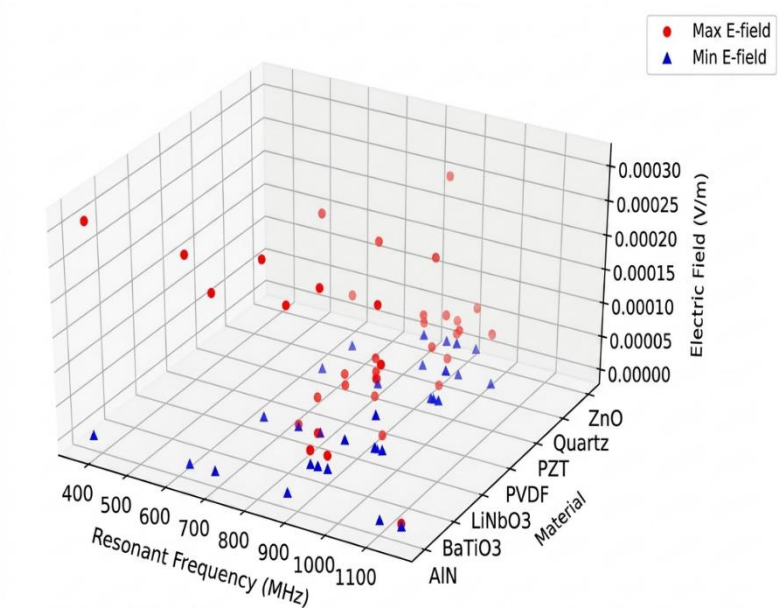

Figure 5. 3D electric field vs. resonant frequency

The figure-5 shown above shows the 3D plot showing the relationship between resonant frequency (MHz) on x-axis, material on y-axis categorically encoded and electric field on the z-axis. Red dots indicate maximum electric field and it is evident that LiNbO3, quartz, PZT and PVDF have strong electric field generation at different frequency levels. Zinc oxide material has medium values over wide frequency range while minimum electric fields are exhibited by PVDF and BaTiO3. Light blue triangles show weak coupling at certain frequencies.

Above figure-6 shows the scatter plot of resonant frequency versus maximum electric field for each piezoelectric material used in the SAW device. Aluminum nitride produced higher electric field at lower and higher resonant frequencies while LiNbO3, Quartz and PZT had similar strong electric fields clustering around (800-950) MHz. ZnO shows moderate electric fields across wide frequency span.

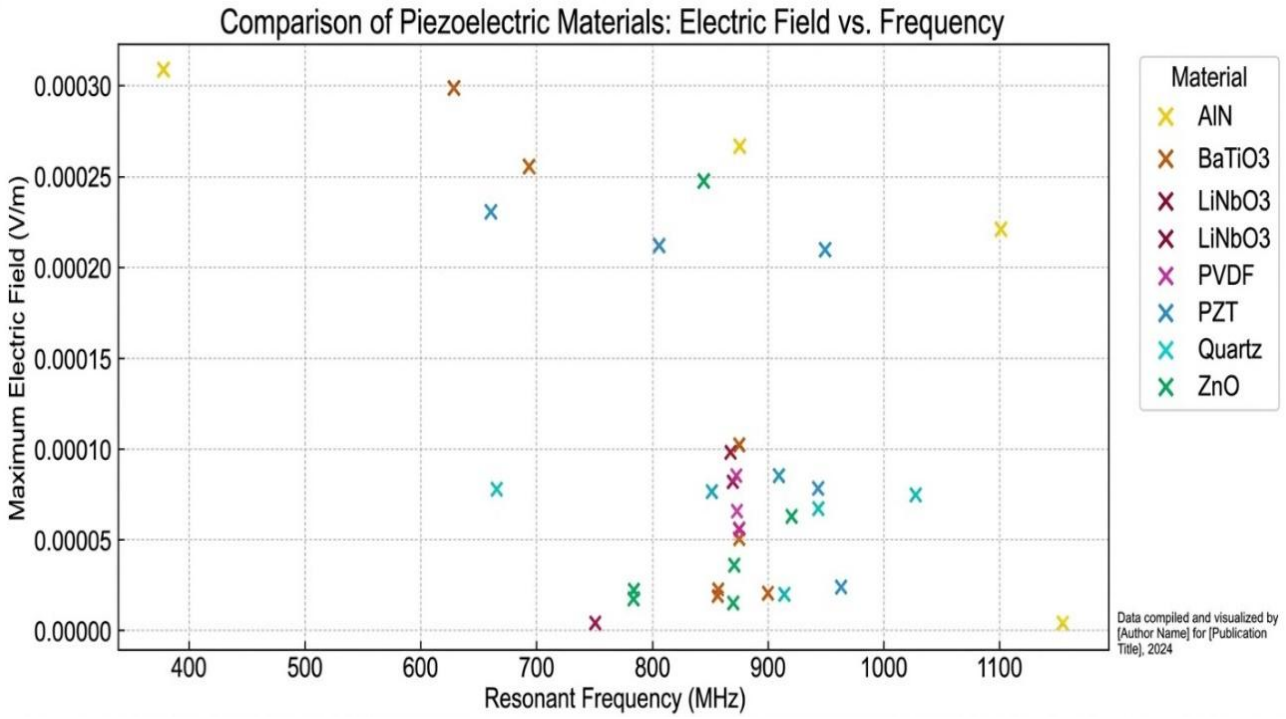

Figure 6. Resonant frequency Vs maximum electric field response graph

3.3 Electric Potential Characteristics

In a surface acoustic wave (SAW) device using piezoelectric material the estimation and analysis of electric potential is crucial for understanding the device performance and optimizing its characteristics [40]. The electric potential distribution helps visualize how effectively the electric field couples with the acoustic wave in the piezoelectric substrate [41]. The electric potential analysis helps to optimize IDT finger spacing, the IDT finger geometry and the number of fingers [42].

Also, it is possible to identify different wave modes like Rayleigh, sezawa [43]. The interaction of the surface with external stimuli (gas) affects the wave propagation. The electric potential distribution is directly related with the SAW device sensitivity as it estimates how surface perturbations affects signal response [44]. In this research work nine different piezoelectric materials are taken and electric potential analysis is done. The analysis helps to compare performance guiding the selection of most suitable material for specific frequency applications [45]. The analysis indicate manufacturing defects, electrode misalignment or any inhomogeneity in the substrate [46].

Thus, an electric potential analysis helps to validate the design of a SAW device making it essential for both simulation and experimental development of SAW devices. + 5 shows the minimum and maximum surface electric potential exhibited by the different piezoelectric materials used in the designed SAW device. From the observed values it is found that AlN, ZnO and Quartz have consistent surface electric potential of 1.31×10^{-11} V while $BaTiO_3$ and PZT have the same level of voltage with some variations.

Symmetric potential distribution is seen in few of the piezoelectric materials while others exhibit asymmetric behaviour which can be due to built-in electric fields, material domain orientations, crystal structure anisotropy and surface charge accumulation effects. An unusually zero surface potential exist in rochelle salt and GaAs which are caused due to the crystal structure changes due to environmental conditions. The consistent value of 1.31×10^{-11} V suggest that for the designed SAW device, this might represent a fundamental limit which can be related due to mesh resolution limits, standardized excitation conditions and other parametric constraints.

Figure 7 shows the electric potential simulation result of $LiNbO_3$ based piezoelectric SAW device at 805.6 MHz. The positive electric potential is indicated by red while blue colored region indicates the negative electric potential. The white/gray portion is the neutral or near-zero potential. The two alternating prominent lobes with peaks suggest the presence of strong electric field concentration under the interdigitated transducer (IDT) region. Below these regions the potential diminishes fast indicating localization of wave energy.

Based on the consistency and high frequency applications AlN can be preferred. Though PZT showed consistent results with meager variations, they are used for actuator applications. As PVDF has shown large scale variability in surface potential, they are suitable for flexible applications despite inconsistency. The piezoelectric materials showing asymmetric surface potential characteristics can require bias compensation circuits [47] while frequency independent materials specify broadband device design. The analysis reveals

that most of the simulated piezoelectric materials show similar maximum surface potential magnitudes. The observed values shows that for SAW sensors with increased sensitivity, $LiNbO_3$ or PZT can be used while PVDF has high variability within the SAW device proximity which is suitable for flexible applications despite inconsistency.

Table 5. Maximum and minimum electric potential in the SAW device

Material	Resonant frequency (MHz)	Maximum voltage	Minimum Voltage
Aluminium Nitride (AlN)	378	$1.31x10^{-11}$ V	$-1.31x10^{-11}$ V
	628	$1.31x10^{-11}$ V	$-1.31x10^{-11}$ V
	693	$1.31x10^{-11}$ V	$-1.31x10^{-11}$ V
	875	$1.31x10^{-11}$ V	$-1.31x10^{-11}$ V
	1101	$1.31x10^{-11}$ V	$1.31x10^{-11}$ V
	1154	$-3.71x10^{-14}$ V	$1.31x10^{-12}$ V
Barium Titanate ($BaTiO_3$)	856.03	$1.31x10^{-11}$ V	$-1.13x10^{-11}$ V
	856.24	$1.31x10^{-11}$ V	$-1.13x10^{-11}$ V
	874.54	$1.31x10^{-11}$ V	$-1.31x10^{-11}$ V
	874.74	$1.31x10^{-11}$ V	$-5.89x10^{-12}$ V
	899.1	$1.31x10^{-11}$ V	$-1.31x10^{-11}$ V
	899.3	$1.31x10^{-11}$ V	$-1.29x10^{-11}$ V
Gallium Arsenide (GaAs)	822.93	0 V	0 V
	822.95	0 V	0 V
	864.14	0 V	0 V
	865.52	0 V	0 V
	879.09	0 V	0 V
	892.87	0 V	0 V
Lithium Niobate ($LiNbO_3$)	660.35	$1.31x10^{-11}$ V	$-1.31x10^{-11}$ V
	750.06	$1.31x10^{-11}$ V	0 V
	805	$1.31x10^{-11}$ V	$-1.31x10^{-11}$ V
	942.76	$1.31x10^{-11}$ V	$-1.31x10^{-11}$ V
	948.59	$1.31x10^{-11}$ V	$-2.99x10^{-12}$ V
	962	$1.31x10^{-11}$ V	$-2.99x10^{-12}$ V
Polyvinylidene fluoride (PVDF)	867.19	$1.31x10^{-11}$ V	$-1.31x10^{-11}$ V
	868.93	$1.31x10^{-11}$ V	$-1.26x10^{-11}$ V
	872.1	$1.31x10^{-11}$ V	$-1.31x10^{-11}$ V
	872.8	$1.31x10^{-11}$ V	$-6.65x10^{-12}$ V
	873.23	$1.31x10^{-11}$ V	$-1.31x10^{-11}$ V
	875.65	$1.31x10^{-11}$ V	$-8.74x10^{-12}$ V
Lead Zirconate Titanate (PZT)	660.35	$1.31x10^{-11}$ V	$-1.31x10^{-11}$ V
	750.64	$1.31x10^{-11}$ V	$-1.31x10^{-11}$ V
	805.63	$1.32x10^{-11}$ V	$-1.32x10^{-11}$ V
	942.76	$1.31x10^{-11}$ V	$-1.31x10^{-11}$ V
	948.59	$1.31x10^{-11}$ V	$-1.31x10^{-11}$ V
	962.47	$1.31x10^{-11}$ V	$-2.99x10^{-12}$ V
Quartz	665.3	$1.31x10^{-11}$ V	$-1.86\ x10^{-12}$ V
	850.85	$1.31x10^{-11}$ V	$-1.83x10^{-12}$ V
	908.84	$1.31x10^{-11}$ V	$-1.31x10^{-11}$ V
	913.66	$1.31x10^{-11}$ V	$-5.57x10^{-13}$ V
	943.16	$1.31x10^{-11}$ V	$-1.31x10^{-11}$ V
	1027	$1.31x10^{-12}$ V	$-1.77x10^{-11}$ V
Rochelle salt	841.7	0 V	0 V
	841.8	0 V	0 V
	862.04	0 V	0 V
	863.84	0 V	0 V
	877.61	0 V	0 V
	891.94	0 V	0 V
ZnO	783.15	$1.31x10^{-11}$ V	$-8.75x10^{-12}$ V
	783.53	$1.31x10^{-11}$ V	$-1.31x10^{-11}$ V
	843.45	$1.32x10^{-11}$ V	$-1.32x10^{-11}$ V

	869.64	$1.31x10^{-11}$ V	$-6.22x10^{-12}$ V
	870.24	$1.31x10^{-11}$ V	$-1.31x10^{-11}$ V
	920.19	$1.31x10^{-11}$ V	$-2.54x10^{-14}$ V

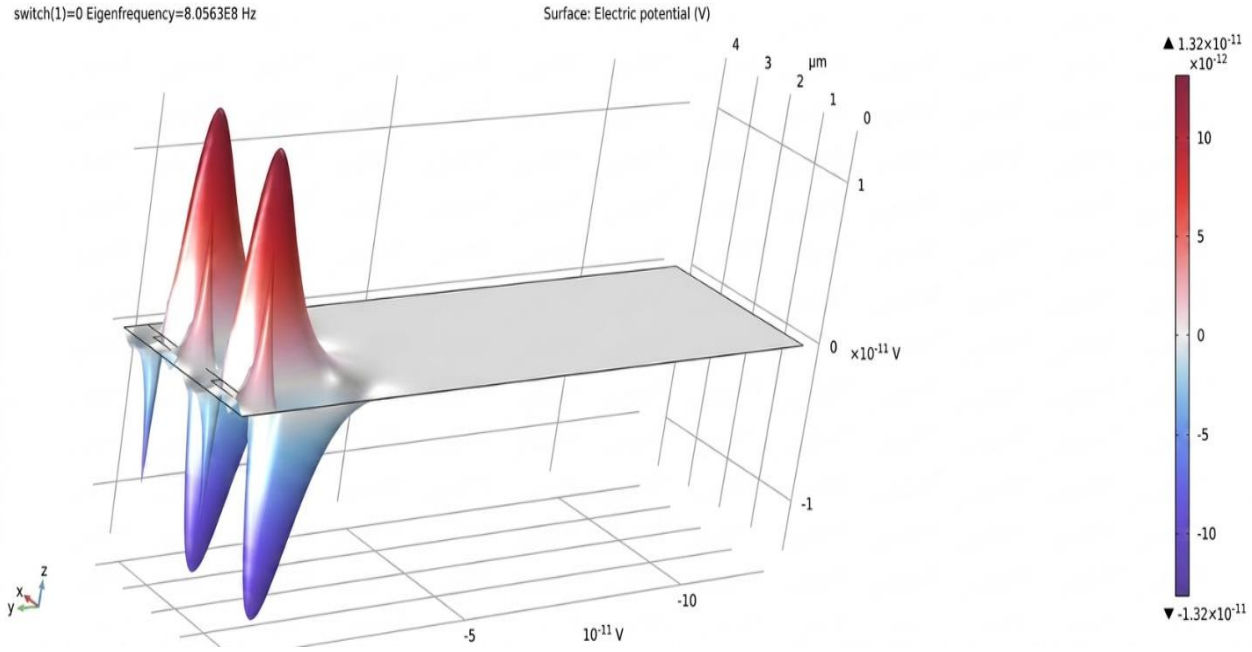

Figure 7. Electric potential of the $LiNbO_3$-based SAW device at 805.6 MHz

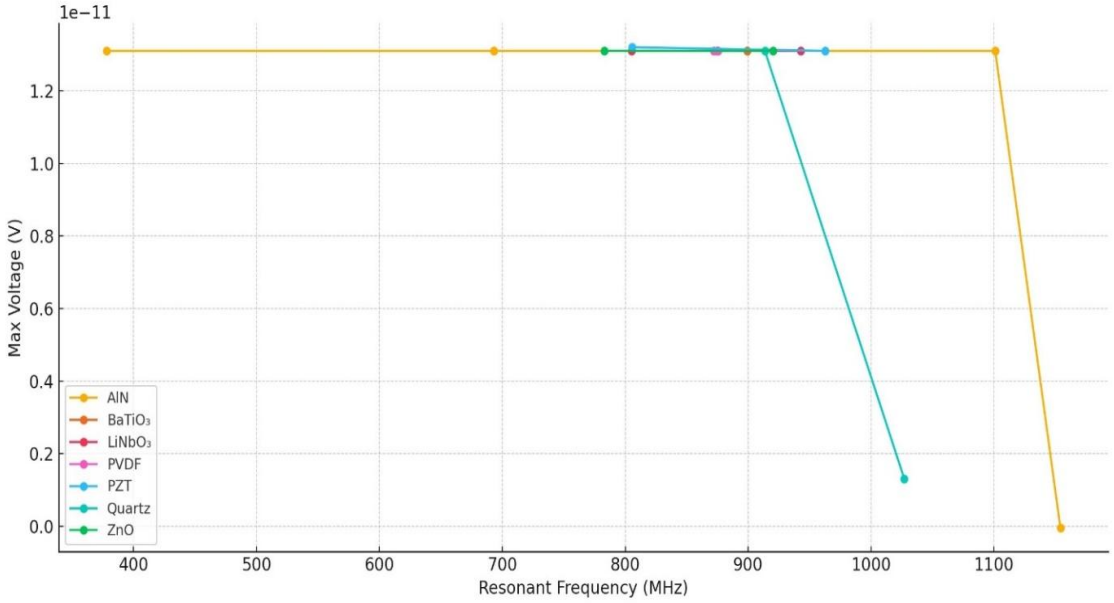

Figure 8. Maximum voltage vs. resonant frequency for different piezoelectric materials

From the (figure 8) graph-8 it is observed that quartz SAW device provided a constant response but produced a notable drop in surface electric potential at higher frequencies. AlN indicated a surprisingly low value at 1154 MHz resonant frequency that is due to material non-linearity [48]. The inference from the plot is that while frequency affects the output electric potential to a certain extent, the material properties dominate the generation of electric potential at the surface of the SAW devices.

From the figure 9 bar chart representation, it is evident that amongst the piezoelectric material used, AlN, ZnO, $LiNbO_3$ and $BaTiO_3$ exhibit strong and symmetric voltage (± $1.3x10^{-11}$ V) which is a good indicator of excellent piezoelectric property. PVDF and ZnO exhibited slightly deeper minimum voltages that are applied in applications desiring higher sensitivity.

The 3D chart illustrating maximum voltage (blue) and minimum voltage (red) values with respect to

resonant frequency (MHz) at X-axis and piezoelectric materials at the Y-axis is shown in figure 10. From the figure it is noticed that quartz and ZnO exhibited greater variation between maximum and minimum, indicating dynamic variation between maximum and minimum indicating dynamic piezoelectric responses. PZT, PVDF, $LiNbO_3$ and AlN exhibited constant maximum voltages. It is also observed that there is a separation between blue and red point pairs for each material that indicates the voltage swing that is important for applications requiring high signal output. To support the validity of the simulated electrical results, the electric-potential and electric-field distributions were compared with representative recent SAW literature. $LiNbO_3$ showed a stronger non-zero electrical response than quartz, which is consistent with reported electroacoustic coupling trends in SAW devices [49, 50].

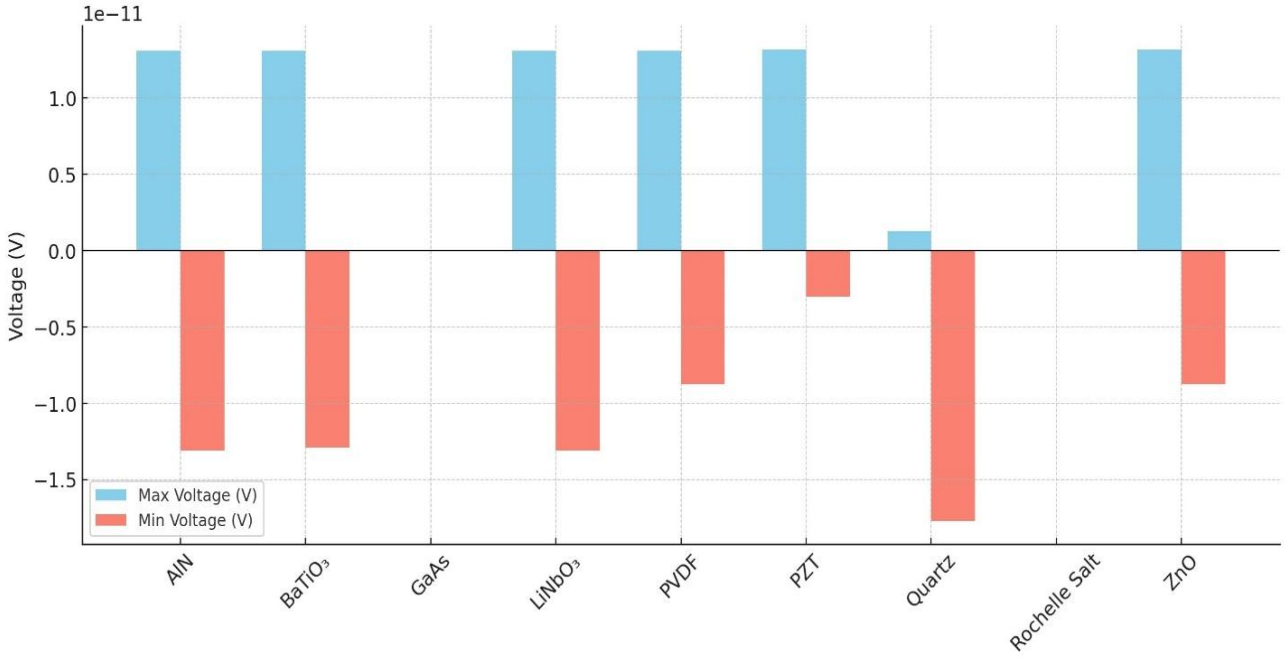

Figure 9. Bar chart representing maximum and minimum voltages

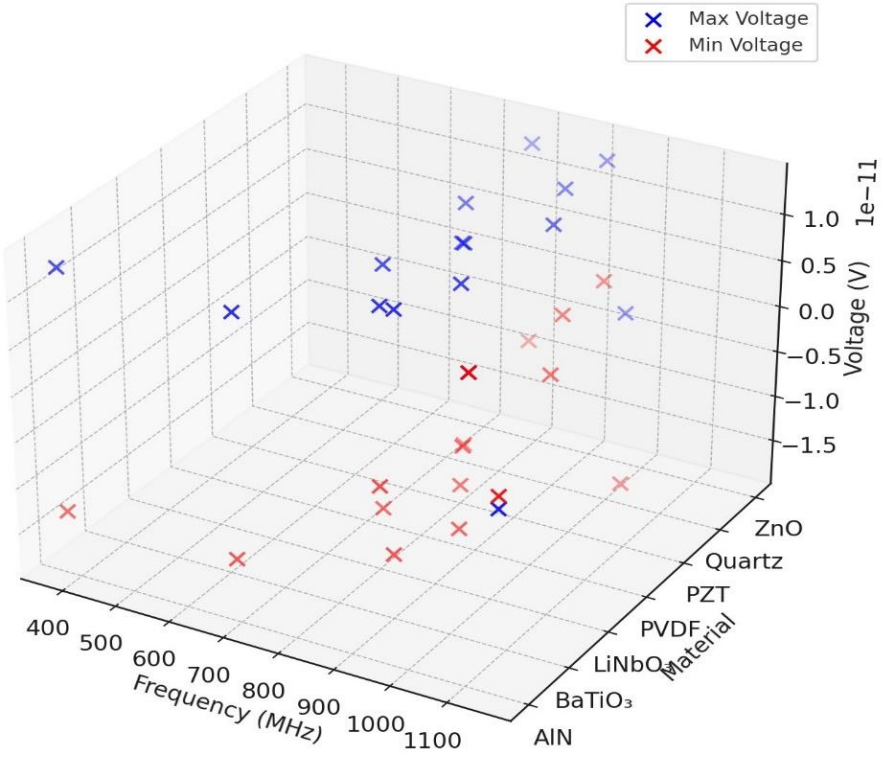

Figure 10. 3D plot of electric potential, resonant frequency response of SAW device

ZnO likewise exhibited non-zero mode-dependent electrical distributions, in agreement with published acoustoelectric FEM studies of Rayleigh and Sezawa waves [51]. AlN also demonstrated an electrically active response consistent with reported AlN-based SAW resonator behavior [52].

4. Key Inferences and Impact

The present results indicate that substrate selection produces distinct operating regimes even when the same SAW geometry and boundary conditions are maintained. In the current configuration, $LiNbO_3$, PZT, PVDF and quartz behave as broad response substrates because they retain non-zero electric fields across relatively wide resonant-frequency ranges. By contrast, ZnO, $BaTiO_3$ and AlN shift the response toward comparatively higher-frequency operation, although with greater variation in field magnitude between modes.

GaAs and Rochelle salt yield zero electric field and zero electric potential in the present model and are therefore not promising for surface-potential generation in this device configuration. These findings are consistent with earlier SAW gas-sensor studies, but extend them to a broader materials framework. Moustafa et al. compared ZnO and $LiNbO_3$ substrates for a PIB-coated DCM SAW gas sensor and reported substrate-dependent resonance behavior [53]. The present work extends that idea by comparing nine piezoelectric materials under one common model structure. Similarly, recent studies have typically focused on optimizing a single substrate platform, such as $LiNbO_3$-based VOC SAW sensing [54] or AlN/diamond/Si multilayer SAW gas sensing [55], whereas the present study emphasizes the earlier design-stage question of substrate selection itself.

The present results also complement recent modeling and review studies that emphasize parameter sensitivity, resonator integration, and sensor application scope [56-58]. In this sense, the present work contributes a practical material-screening step that can guide later optimization of coating thickness, circuit interfacing, uncertainty analysis, and fabrication strategy.

5. Conclusion

Surface acoustic wave (SAW) device using nine different piezoelectric materials for gas sensing application is designed and investigated for its electrical characteristics like electric field and electric potential at different resonant frequency values. As far as electric field is concerned, piezoelectric materials $LiNbO_3$, PZT, PVDF and Quartz exhibited high electric fields with good resonant frequency response which indicates high sensitivity over a wide frequency range compatibility. Also, from the results it is observed that ZnO, $BaTiO_3$ and AlN has moderate electric fields but at high frequency applications. Both electric field and electric potential observations for rochelle salt and GaAs resulted in zero values likely due to weak piezoelectric coupling for gas input. This infers that they are not suitable for surface potential generation. The simulated resonant frequencies span about 378.2–1154.5 MHz with AlN showing the highest reported resonance (1154.5 MHz), while $LiNbO_3$/PZT cover 660.35–962.47 MHz, quartz covers 665.3–1027 MHz, and ZnO covers 783.15–920.19 MHz. Symmetric voltage responses are observed in many of the materials showing strong electrical oscillations primarily caused by mechanical displacement of the surface when subjected to gas. The presented work will contribute to a significant extent for the future development of optimal design of piezoelectric SAW device for gas sensing applications.

References

[1] Z. Zhou, H. Wang, L. Lou, Design and Characterization of Surface Acoustic Wave-Based Wireless and Passive Temperature Sensing System. Micromachines, 15(4), (2024) 544. https://doi.org/10.3390/mi15040544

[2] V.S. Sreejith, H. Zhang, Modeling and Testing of a Highly Sensitive Surface Acoustic Wave Pressure Sensor for Liquid Depth Measurements. Sensors and Actuators A: Physical, 372, (2024) 115377. https://doi.org/10.1016/j.sna.2024.115377

[3] Y. Dou, C. Li, W. Luo, L. Qian, L. Wang, D. Li, H. Li, M. Li, Surface Acoustic Wave Relative Humidity Sensor Based on GO/TiO_2 Sensitive Film. Sensors and Actuators A: Physical, 365, (2024) 114906, https://doi.org/10.1016/j.sna.2023.114906

[4] F. Chen, J. Lu, S. Liang, Y. Otani, X. Yang, Y. Zhang, W. Luo, Widen-Dynamic-Range Surface Acoustic Wave Magnetic Sensors with High Sensitivity. Journal of Alloys and Compounds, 980, (2024) 173635. https://doi.org/10.1016/j.jallcom.2024.173635

[5] A. Ntimtsas, E. Gizeli, Portable Surface Acoustic Wave Device Platform Coupled with a Paper-Based Capillary Fluidics for Real-Time Biosensing Applications. Sensors and Actuators A: Physical, 378, (2024) 115814. https://doi.org/10.1016/j.sna.2024.115814

[6] Y. Pan, C. Yan, X. Gao, J. Yang, T. Guo, L. Zhang, W. Wang, A Passive Wireless Surface Acoustic Wave (SAW) Sensor System for Detecting Warfare Agents Based on Fluoroalcohol Polysiloxane Film. Microsystems & Nanoengineering, 10(1), (2024) 4. https://doi.org/10.1038/s41378-023-00627-8

[7] L. Bo, J. Li, Z. Wang, C. Qiu, B. Cai, Y. Du, T. Li, H. Liu, Z. Tian, Frequency-Locked Wireless Multifunctional Surface Acoustic Wave Sensors. Advanced Sensor Research, *3*(12), (2024) 2400083. https://doi.org/10.1002/adsr.202400083

[8] S.Y. Shevchenko, D.A. Mikhailenko, A.S. Kukaev, V.Y. Venediktov, Circular SAW Resonators: Influence of Sensitive Element Dimensions on Strength Characteristics and First Experimental Samples. Sensors, 24(14), (2024) 4584. https://doi.org/10.3390/s24144584

[9] Z. Xiang, Q. Liu, F. Huang, T. Wang, W. Zhang, A Responsive Viscosity Sensing System with a Flow Channel Based on a One-Port Resonator. Sensors and Actuators A: Physical, 365, (2024) 114873. https://doi.org/10.1016/j.sna.2023.114873

[10] Y.B. Chu, Performance Analysis of Shear Horizontal One Port Surface Acoustic Wave (SAW) Resonator for Optimal Liquid Sensing Based on Finite Element Method. E-Prime-Advances in Electrical Engineering, Electronics and Energy, 10, (2024) 100799. https://doi.org/10.1016/j.prime.2024.100799

[11] X. Meng, Z. Li, Design and Analysis of Interdigital Electrode Parallel Layout of Multilayer SAW Devices. IEEE Access, IEEE, 12, (2024) 43453-43459. https://doi.org/10.1109/ACCESS.2024.3380370

[12] N. Ramakrishnan, H.B. Nemade, R.P. Palathinkal, Resonant Frequency Characteristics of a SAW Device Attached to Resonating Micropillars. Sensors. 12(4), (2012) 3789-3797. https://doi.org/10.3390/s120403789

[13] S.R. Karbari, M.U. Kumari, G. Shireesha, Modelling and Optimization of PVDF based Surface Acoustic Wave MEMS Microphone. Materials Today: Proceedings, 46(Part 6), (2021) 2255-2260. https://doi.org/10.1016/j.matpr.2021.03.589

[14] L. Tongbin, C. Shien, Z. Ning, K. Xin, Research on SAW Sensors in TPMS. In2017 4th International Conference on Information Science and Control Engineering (ICISCE), IEEE, Changsha, China. https://doi.org/10.1109/ICISCE.2017.348

[15] S. Qureshi, M. Hanif, V. Jeoti, G.M. Stojanović, M.T. Khan, Review of Fabrication of SAW Sensors on Flexible Substrates: Challenges and Future. Results in Engineering, 22, (2024) 102323. https://doi.org/10.1016/j.rineng.2024.102323

[16] C. Jiang, Y. Chen, C. Cho, A Three-Dimensional Finite Element Analysis Model for SH-SAW torque Sensors. Sensors, 19(19), (2019) 4290. https://doi.org/10.3390/s19194290

[17] M.M. Memon, S. Pan, J. Wan, T. Wang, B. Peng, W. Zhang, Sensitivity Enhancement of SAW Pressure Sensor based on the Crystalline Direction. IEEE Sensors Journal, IEEE, 22(10), (2022) 9329-35. https://doi.org/10.1109/JSEN.2022.3165623

[18] G.S. Wood, I. Gual, P. Parmiter, R. Cheung, Temperature Stability of Electro-Thermally and Piezoelectrically Actuated Silicon Carbide MEMS Resonators. Microelectronics Reliability, 50(12), (2010), 1977-1983. https://doi.org/10.1016/j.microrel.2010.05.011

[19] G.A. Borrero, J.P. Bravo, S.F. Mora, S. Velásquez, F.E. Segura-Quijano, Design and Fabrication of SAW Pressure, Temperature and Impedance Sensors using novel multiphysics Simulation Models. Sensors and Actuators A: Physical, 203, (2013) 204-214. https://doi.org/10.1016/j.sna.2013.08.021

[20] R. Patel, V.K. Agrawal, D. Boolchandani, K.J. Rangra, Design of MEMS based Film Bulk Acoustic Wave Resonator. Materials Today: Proceedings, 4(9), (2017) 10377-82. https://doi.org/10.1016/j.matpr.2017.06.384

[21] J. Zhang, H. Jin, J. Chen, W. Xuan, R. Ding, S. Dong, J. Luo, High Temperature effects on Surface Acoustic Wave Strain Sensor. Sensors and Actuators A: Physical, 338, (2022) 113464. https://doi.org/10.1016/j.sna.2022.113464

[22] A. Assali, F. Laidoudi, R. Serhane, F. Kanouni, O. Mezilet, Highly enhanced electro-acoustic properties of YAlN/sapphire based surface acoustic wave devices for next generation of microelectromechanical systems. Materials Today Communications. 26, (2021) 102067. https://doi.org/10.1016/j.mtcomm.2021.102067

[23] J. Yanez, A. Uranga, N. Barniol, Fluid Compressional Properties Sensing at Microscale using a Longitudinal Bulk Acoustic Wave Transducer Operated in a Pulse-Echo Scheme. Sensors and Actuators A: Physical, 334, (2022) 113334. https://doi.org/10.1016/j.sna.2021.113334

[24] D. Kong, K. Nishio, M.K. Kurosawa, Surface Acoustic Wave Propulsion System with Acoustic Radiation Force. Sensors and Actuators A: Physical, 309, (2020) 111943. https://doi.org/10.1016/j.sna.2020.111943

[25] A. Kumar, G. Thachil, S. Dutta, Ultra High Frequency Acoustic Wave Propagation in Fully

Polymer based Surface Acoustic Wave Device. Sensors and Actuators A: Physical, 292, (2019) 52-9. https://doi.org/10.1016/j.sna.2019.03.023

[26] K. Wang, W. Zhou, Z. Lin, F. Cai, F. Li, J. Wu, L. Meng, L. Niu, H. Zheng, Sorting of Tumour Cells in a Microfluidic Device by Multi-Stage Surface Acoustic Waves. Sensors and Actuators B: Chemical, 258, (2018) 1174-83. https://doi.org/10.1016/j.snb.2017.12.013

[27] S. Karamdoust, Functionalized Polyisobutylene: From Synthesis to Properties and Applications. The University of Western Ontario (Canada), ProQuest Dissertations & Theses, (2013) 29241430. https://www.proquest.com/openview/632c982d06e4daf4714fdaed96e48059/1?pq-origsite=gscholar&cbl=18750&diss=y

[28] K. Kunal, M. Paluch, C.M. Roland, J.E. Puskas, Y. Chen, A.P. Sokolov, Polyisobutylene: A most unusual polymer. Journal of Polymer Science Part B: Polymer Physics, 46(13), (2018) 1390-1399. https://doi.org/10.1002/polb.21473

[29] J.J. Higgins, F.C. Jagisch, N.E. Stucker, Butyl Rubber and Polyisobutylene. In Handbook of Adhesives, Boston, MA: Springer US, (1990) 185-205. https://doi.org/10.1007/978-1-4613-0671-9_10

[30] E.R. Fitzgerald, L.D. Grandine Jr, JD. Ferry, Dynamic Mechanical Properties of Polyisobutylene. Journal of Applied Physics, 24(5), (1953) 650-655. https://doi.org/10.1063/1.1721345

[31] K. Ren, M. Zhang, J. He, Y. Wu, P. Ni, Preparation of polymeric Prodrug Paclitaxel-Poly (Lactic Acid)-*b*-Polyisobutylene and its Application in Coatings of a Drug Eluting Stent. ACS Applied Materials & Interfaces, 7(21), (2015) 11263-71. https://doi.org/10.1021/acsami.5b01410

[32] M. Kumar, D. Bhadu, Design Performance and Frequency Response Analysis of SAW-Based Sensor for Dichloromethane Gas Sensing Amidst the COVID-19. Journal of Vibration Engineering & Technologies, 9(5), (2021) 725-732.https://doi.org/10.1007/s42417-020-00257-8

[33] B. Frick, D. Richter, Change of the Vibrational Dynamics near the Glass Transition in Polyisobutylene: Inelastic Neutron Scattering on a Nonfragile Polymer. Physical Review B, 47(22), (1993) 14795. https://doi.org/10.1103/PhysRevB.47.14795

[34] P. Olafsson, R. Sandstrom, Å. Karlsson, Comparison of Experimental, Calculated and Observed Values for Electrical and Thermal Conductivity of Aluminium Alloys. Journal of Materials Science, 32(16), (1997) 4383-90. https://doi.org/10.1023/A:1018680024876

[35] M.Z. Aslam, V. Jeoti, S. Karuppanan, A.F. Malik, A. Iqbal, FEM Analysis of Sezawa Mode SAW Sensor for VOC Based on CMOS Compatible AlN/SiO_2/Si Multilayer Structure. Sensors. 18(6), (2018) 1687. https://doi.org/10.3390/s18061687

[36] L. Zheng, D. Wu, X. Wu, K. Lai, Visualization of Surface-Acoustic-Wave Potential by Transmission-Mode Microwave Impedance Microscopy. Physical Review Applied, 9(6), (2018) 061002. https://doi.org/10.1103/PhysRevApplied.9.061002

[37] S. Fu, W. Wang, Q. Li, Z. Lu, Z. Chen, J. Luo, J. Shen, R. Wang, C. Song, F. Zeng, F. Pan, High-frequency V-doped ZnO/SiC surface acoustic wave devices with enhanced electromechanical coupling coefficient. Applied Physics Letters, 114(11), (2019), 113504. https://doi.org/10.1063/1.5086445

[38] A. Chauhan, R. Vaish, Material Selection for Piezoelectric Devices. Advanced Science, Engineering and Medicine, 5(7), (2013) 715-719. https://doi.org/10.1166/asem.2013.1285

[39] R.D. Janardhana, N. Jackson, A Simulated Investigation of Lithium Niobate Orientation Effects on Standing Acoustic Waves. Sensors, 23(19), (2023) 8317. https://doi.org/10.3390/s23198317

[40] M. Hofer, N. Finger, G. Kovacs, J. Schoberl, S. Zaglmayr, U. Langer, R. Lerch, Finite-Element Simulation of Wave Propagation in Periodic Piezoelectric SAW Structures. IEEE Transactions on Ultrasonics, Ferroelectrics, and Frequency Control, IEEE, 53(6), (2006) 1192-201. https://doi.org/10.1109/TUFFC.2006.1642518

[41] H. Xu, S. Fu, R. Su, J. Shen, F. Zeng, C. Song, F. Pan, Enhanced Coupling Coefficient in Dual-Mode ZnO/SiC Surface Acoustic Wave Devices with Partially Etched Piezoelectric Layer. Applied Sciences, 11(14), (2021) 6383. https://doi.org/10.3390/app11146383

[42] Z. Wang, T. Tang, S. Chen, B. Chen, Field Analysis and Calculation of Interdigital Transducers with Arbitrary Finger Shapes. Journal of Physics D: Applied Physics, 39(22), (2006) 4902–4908. https://doi.org/10.1088/0022-3727/39/22/024

[43] C.K. Kent, N. Ramakrishnan, H.P. Kesuma, Advancements in One-Port Surface Acoustic

Wave (SAW) Resonators for Sensing Applications: A review. IEEE Sensors Journal, IEEE, 24(11), (2024) 17337-52. https://doi.org/10.1109/JSEN.2024.3386917

[44] L. Yang, E. Zappino, E. Carrera, J. Du, Rotation effects on Propagation of Shear Horizontal Surface Waves in Piezomagnetic-Piezoelectric Semiconductor Layered Structures. Applied Mathematical Modelling, 129, (2024) 494-508. https://doi.org/10.1016/j.apm.2024.02.020

[45] R. Kumar, N. Mandal, SAW Sensor basics on Material, Antenna, and Applications: a Review. IEEE Sensors Journal, 24(5), (2024) 5713-31. https://doi.org/10.1109/JSEN.2024.3349656

[46] M. Li, Z. Liu, K. Huang, Y. He, X. Xia, K. Li, K. Chen, G. Tang, Analysis Method for the Influence of Parasitic Surface Conductivity on Silicon-based Surface Acoustic Wave Devices. IEEE Transactions on Electron Devices, 71(6), (2024) 3478-82. https://doi.org/10.1109/TED.2024.3386876

[47] J. Liao, P. Li, J. Ma, R. Li, Z. Gao, X. Zhuang, Low Noise Feed-Through Compensation Circuit Design for Resonant MEMS Pressure Sensor. Micromachines, 16(4), (2025) 400. https://doi.org/10.3390/mi16040400

[48] J.A. Boales, S. Erramilli, P. Mohanty, Measurement of nonlinear piezoelectric coefficients using a micromechanical resonator. Applied Physics Letters, 113(8), (2018) 083501.https://doi.org/10.1063/1.5041375

[49] Y. Liu, K. Liu, J. Li, Y. Li, T. Wu, Spurious-Free Shear Horizontal Wave Resonators Based on 36Y-Cut $LiNbO_3$ Thin Film. Micromachines, 15(4), (2024) 477. https://doi.org/10.3390/mi15040477

[50] C. Caliendo, M. Benetti, D. Cannatà, F. Laidoudi, G. Petrone, Interface Acoustic Waves in 128° YX-$LiNbO_3$/SU-8/Overcoat Structures. Micromachines, 16(1), (2025) 99. https://doi.org/10.3390/mi16010099

[51] C. Caliendo, Acoustoelectric Effect of Rayleigh and Sezawa Waves in ZnO/Fused Silica Produced by an Inhomogeneous In-Depth Electrical Conductivity Profile. Sensors, 23(6), (2023) 2988. https://doi.org/10.3390/s23062988

[52] M. Kwon, I. Ignat, D. Platz, H. Arthaber, U. Schmid, Aluminum nitride surface acoustic wave resonators with high Qf product by optical lithography. Sensors and Actuators A: Physical, 362, (2023) 114637. https://doi.org/10.1016/j.sna.2023.114637

[53] M. Moustafa, G. Laouini, T. Alzoubi, Finite Element Analysis of SAW Sensor with ZnO Substrate for Dichloromethane (DCM) Gas Detection. Archives of Acoustics, 46(3), (2021) 419–426. https://doi.org/10.24425/aoa.2021.138135

[54] A. Tiwary, J. Kumar, B. Behera, Analysis of CNT-based SAW sensor for the detection of volatile organic compounds. Physica B: Condensed Matter, 669, (2023) 415279. https://doi.org/10.1016/j.physb.2023.415279

[55] Z. Abu Waar, M. Moustafa, Design and Analysis of SAW Gas Sensor Utilizing AlN/Diamond/Si Multilayered Structure for VOCs Detection. Journal of Electronic Materials, 53, (2024) 5255–5264. https://doi.org/10.1007/s11664-024-11282-8

[56] M. Hamdaoui, Uncertainty Propagation and Global Sensitivity Analysis of a Surface Acoustic Wave Gas Sensor Using Finite Elements and Sparse Polynomial Chaos Expansions. Vibration, 6(3), (2023) 610–624. https://doi.org/10.3390/vibration6030038

[57] M. Z. Aslam, H. Zhang, V.S. Sreejith, M. Naghdi, S. Ju, Advances in the surface acoustic wave sensors for industrial applications: Potentials, challenges, and future directions: A review. Measurement, 222, (2023)113657. https://doi.org/10.1016/j.measurement.2023.113657

[58] S.G. Ramaraj, A. Alrebh, D. Elamaran, H. Zhou, K. Huang, M. Almansoori, H. Yamahara, H. Tabata, Surface Acoustic Wave Gas Sensors: Recent Developments and their Role in Sensing Technology. Materials Science and Engineering: B, 317, (2025) 118157. https://doi.org/10.1016/j.mseb.2025.118157

Authors Contribution Statement

S. Bestley Joe: Conceptualization, Methodology, Investigation, Formal analysis, Writing - Original Draft. S. Aaron James: Methodology, Investigation, Writing - Review & Editing. S. Maflin Shaby: Writing - Review & Editing. A.S. Augustine Fletcher: Conceptualization, Writing - Review & Editing. All authors have read and agreed to the published version of the manuscript.

Funding

The authors declare that no funds, grants or any other support were received during the preparation of this manuscript.

Competing Interests

The authors declare that there are no conflicts of interest regarding the publication of this manuscript.

Has this article screened for similarity?

Yes

Data Availability

The data supporting the findings of this study can be obtained from the corresponding author upon reasonable request.

About the License

© The Author(s) 2026. The text of this article is open access and licensed under a Creative Commons Attribution 4.0 International License.